Superconductivity in Kagome Metal YRu_3Si_2 with Strong Electron Correlations

Chunsheng Gong(龚春生), Shangjie Tian(田尚杰), Zhijun Tu(涂志俊), Qiangwei Yin(殷蔷薇), Yang Fu(付阳), Ruitao Luo(罗睿韬), and Hechang Lei(雷和畅)*

Laboratory for Neutron Scattering, and Beijing Key Laboratory of Optoelectronic Functional Materials & MicroNano Devices, Department of Physics, Renmin University of China, Beijing 100872, China

(Received 2 June 2022; accepted manuscript online 24 June 2022)

We report the detailed physical properties of YRu_3Si_2 with the Ru kagome lattice at normal and superconducting states. The results of resistivity and magnetization show that YRu_3Si_2 is a type-Ⅱ bulk superconductor with $T_c \sim 3.0$ K. The specific heat measurement further suggests that this superconductivity could originate from the weak or moderate electron-phonon coupling. On the other hand, both large Kadawaki–Woods ratio and Wilson ratio indicate that there is a strong electron correlation effect in this system, which may have a connection with the featured flat band of kagome lattice.

DOI: 10.1088/0256-307X/39/8/087401

It is well known that the kagome lattice provides an exciting platform for studying magnetic frustration, electronic correlation and topological electronic state, due to the unique two-dimensional (2D) structure formed by corner-sharing triangles. Besides the long-sought spin liquid state in insulating magnetic kagome materials with strong geometrical frustration,[1–4] the topological electronic structure in metallic kagome systems (kagome metals), such as Dirac point, flat band and von Hove point rooting in the special symmetry and arrangement of 2D kagome lattice, has also attracted much attention recently.[5–8] More importantly, the interplay between magnetism and band topology has resulted in the emergence of various exotic correlated topological phenomena and matters, such as giant anomalous Hall effect, massive Dirac fermions with large magnetic field tunability, magnetic Weyl semimetal state, and Chern gapped Dirac fermions with chiral edge state.[5,9–15]

In contrast, the experimental studies on other electronic correlation effects intertwining with band topology in kagome metals are scarce due to the lack of material systems. The discovery of superconductivity and CDW state in AV_3Sb_5 (A = K, Rb, Cs) in very recent provide a novel platform to investigate such relationship,[16–19] which has been intensively studied before in theory.[20–23] Moreover, the observed chiral charge order at high temperature and pair density wave state below superconducting transition temperature T_c further imply the intricate relationship between these correlated ordering states and non-trivial band topology.[24,25]

In order to deepen the understanding of such correlated topological phenomena, it is necessary to explore other kagome metals harbouring superconductivity (kagome superconductors) but only a handful of kagome superconductors have been reported until now. One of examples is the Laves phase [cubic $MgCu_2$ (C15) type] superconductors with widely varying T_c ranging from 0.07 K to above 10 K.[26–28] However, since the strong interaction between kagome layer and other layers along the (111) direction of cubic Laves phase, the featured electronic structure of 2D kagome lattice is strongly disturbed and the topological features of these materials become hard to discern. Another family of kagome superconductors is RT_3B_2 (R = Y, La, Lu, Th and T = Ru, Os, Rh, Ir) and RRu_3Si_2 with hexagonal layered $CeCo_3B_2$ structure in which transition metals form kagome layers.[29] Among these materials, $LaRu_3Si_2$ with T_c as high as 7.8 K attracted a great deal of attention because it shows a typical band structure of kagome lattice and strong electron correlations which could be closely related to the kagome flat band.[30–34] When compared with $LaRu_3Si_2$, except the structure and T_c value (∼3–3.5 K),[30,35] the physical properties of YRu_3Si_2, especially superconducting properties, are still lacking. In this work, we carry out a detailed study on the physical properties of YRu_3Si_2 at normal and superconducting states. Experimental results indicate that YRu_3Si_2 is a weakly or moderately coupled BCS superconductor with strong electron correlations.

Experimental. YRu_3Si_2 polycrystal was synthesized using an arc-melting method. First, Y metal filing (99.9%), Ru powder (99.9%), and Si powder (99.9 %) with stoichiometric ratios were mixed, ground thoroughly and then pressed into a pellet using a hydraulic press in a glover box filled with argon atmosphere. In order to avoid the formation of YRu_2Si_2, an extra amount of Ru was added, similar to the preparation of $LaRu_3Si_2$.[32] The pellet was arc-melted under argon atmosphere and remelted several times from both sides of the pellet to improve the homo-

*Corresponding authors. Email: hlei@ruc.edu.cn
© 2022 Chinese Physical Society and IOP Publishing Ltd

geneity. Crystal structure and phase purity were examined by powder x-ray diffraction pattern (PXRD) with Cu K_α radiation ($\lambda = 0.15418$ nm) using a Bruker D8 x-ray diffractometer. The lattice parameters are extracted by fitting the PXRD pattern using the TOPAS4 software.[36] Electrical transport and specific heat measurements were performed in a Quantum Design PPMS-14T. Magnetization measurements were carried out in a Quantum Design MPMS3.

Results and Discussion. Figure 1(a) shows the crystal structure of YRu_3Si_2, isostructural to $LaRu_3Si_2$.[35] It is formed by stacking Y–Si and Ru layers alternately along the c axis. A key feature of this compound is the 2D distorted kagome layer formed by Ru atoms parallel to the ab plane. In this layer, there are two different Ru–Ru bond distances $d_{\mathrm{Ru-Ru}}$ (= 0.2692 nm and 0.2858 nm). Meanwhile, the rotation of Ru triangles leads to the bond angle for collinear Ru atoms θ (= 174.046°) deviating away from $\theta = 180°$ in perfect kagome lattice [Fig. 1(b)]. On the other hand, in the Y–Si layer, the Y atoms form a triangle lattice when the Si atoms construct a honeycomb structure. Figure 1(c) shows the PXRD pattern of YRu_3Si_2 and all peaks can be indexed well by the $P6_3/m$ space group (No. 176). The obtained lattice parameters by using Rietveld refinement are $a = 0.5542(1)$ nm and $c = 0.7150(7)$ nm, consistent with the reported values in the literature.[35] In addition to the diffraction peaks of YRu_3Si_2, there are some extra peaks that originate from the excessive Ru in the raw material. A fitting result shows that the weight ratio of YRu_3Si_2 to Ru is about 84.1 : 15.9.

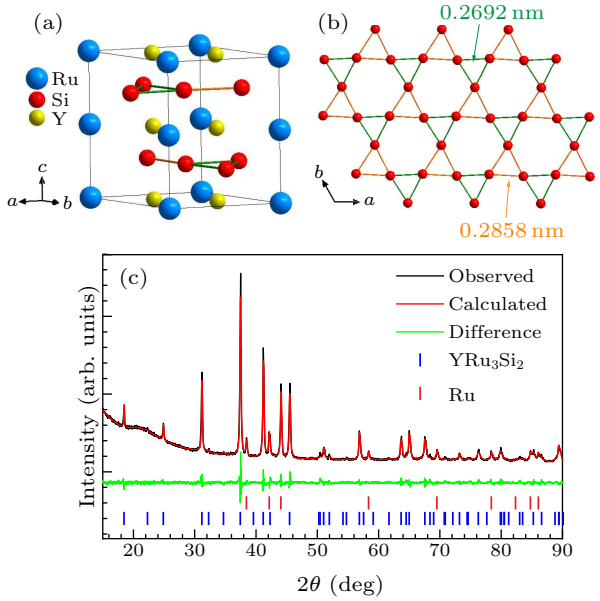

Fig. 1. (a) Crystal structure of YRu_3Si_2. The blue, red and yellow balls represent Y, Ru and Si atoms, respectively. (b) Top view of the 2D distorted kagome lattice of Ru atoms. Two different bond distances are labeled with green and orange lines. (c) Powder XRD pattern and Rietveld refinement of YRu_3Si_2 polycrystal.

The temperature-dependent magnetic susceptibility $4\pi\chi(T)$ with the zero-field cooling (ZFC) and field cooling (FC) modes is shown in Fig. 2(a). A clear diamagnetic transition in the $4\pi\chi(T)$ curve can be observed and confirms the occurrence of superconductivity in YRu_3Si_2. The T_c determined from the ZFC $4\pi\chi(T)$ curve at $\mu_0 H = 1$ mT is about 2.98 K, close to the value reported previously.[30] At $T = 1.8$ K, the estimated superconducting volume fraction is about 110%, indicating a bulk superconductivity in YRu_3Si_2. Compared with the ZFC $4\pi\chi(T)$ curve, a relatively weak diamagnetic signal of FC $4\pi\chi(T)$ curve due to flux pinning effect suggests that YRu_3Si_2 is a type-Ⅱ superconductor. It is further confirmed by the magnetization hysteresis loop measured at 1.8 K [Fig. 2(b)]. Moreover, the sudden jumps of $M(\mu_0 H)$ at low-field region can be ascribed to the entry of Meissner state. The initial magnetization as a function of magnetic field in the temperature range between 1.8 K and 2.9 K is shown in Fig. 2(c). All curves clearly fall on the same line and deviate from linearity at different temperatures. In order to estimate the lower critical field $\mu_0 H_{c1}$ correctly, the effective field $\mu_0 H_{\mathrm{eff}}$ is calculated by using the formula $\mu_0 H_{\mathrm{eff}} = \mu_0 H - N_d M$, where N_d is the demagnetization factor.[37] Using the geometry size of rectangular sample, the calculated value of N_d is about 0.522.[37] The $\mu_0 H_{c1}$ at each temperature is determined from the field where the $4\pi M(\mu_0 H)$ curve deviates from linearity (Meissner line). The obtained $\mu_0 H_{c1}$ as a function of reduced temperature T/T_c is shown in Fig. 2(d). The temperature dependence of $\mu_0 H_{c1}$ can be well fitted by the Ginzburg–Landau (G-L) equation $\mu_0 H_{c1}(T) = \mu_0 H_{c1}(0)[1 - (T/T_c)^2]$, where $\mu_0 H_{c1}(0)$ is the lower critical field at $T = 0$ K (red line). The fitted $\mu_0 H_{c1}(0)$ for YRu_3Si_2 is 28.0(3) mT.

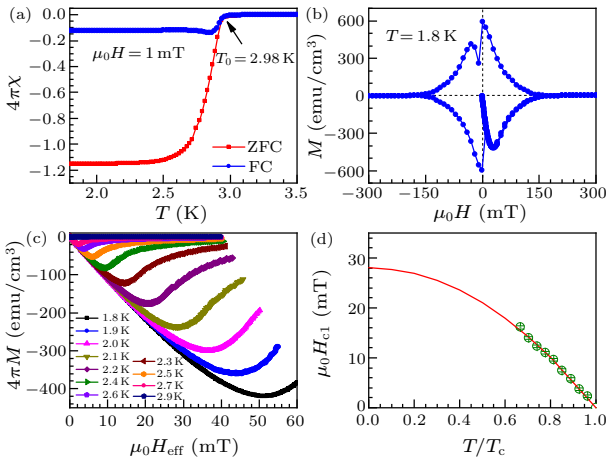

Fig. 2. (a) Temperature dependence of magnetic susceptibility $4\pi\chi(T)$ at 1 mT with ZFC and FC modes. (b) Magnetization hysteresis loop for YRu_3Si_2 at 1.8 K. (c) Low-field dependence of magnetization $4\pi M(\mu_0 H)$ at various temperatures below T_c. (d) Dependence of $\mu_0 H_{c1}$ on T/T_c. The red line represents the fit using G-L equation.

Figure 3(a) shows the temperature dependence of electrical resistivity $\rho(T)$ for YRu_3Si_2 polycrystal from 300 K to 2 K at zero field. The $\rho(T)$ decreases monotonically with decreasing temperature, indicating the metallic behavior of YRu_3Si_2. The value of residual resistivity ratio (RRR) $\rho(300\,\mathrm{K})/\rho(4\,\mathrm{K})$ is about 8.6. Such a relatively

small value of RRR can be explained by the grain boundary effect in YRu_3Si_2 polycrystal. At high temperature the $\rho(T)$ curve exhibits a saturation tendency. This behavior could be described by the Ioffe–Regel limit,[38] e.g., the electron mean free path is close to the interatomic distance.[39] In low temperature region ($T < 30$ K), the $\rho(T)$ curve can be well fitted using the formula $\rho(T) = \rho_0 + AT^2 + BT^5$, where ρ_0 is the residual resistivity, AT^2 and BT^5 term originates from the electron–electron and electron–phonon scattering, respectively (red line). The fit gives $\rho_0 = 4.99(5)\,\mu\Omega\cdot$cm, $A = 2.38(7) \times 10^{-3}\,\mu\Omega\cdot$cm$\cdot$K^{-2} and $B = 5.9(4) \times 10^{-8}\,\mu\Omega\cdot$cm$\cdot$K^{-5}. In addition, because the value of AT^2 is always larger than BT^5 at $T < 30$ K, the electron-electron scattering process dominates low-temperature resistivity. With lowering temperature further, a sharp superconducting transition can be observed at $T_{c,onset} = 3.0$ K with narrow transition width $\Delta T_c = 0.082$ K [inset of Fig. 3(a)]. It is consistent with T_c obtained from the $4\pi\chi(T)$ curve. The small value of ΔT_c indicates the high quality of YRu_3Si_2 polycrystal.

In order to investigate the upper critical field $\mu_0 H_{c2}$ in YRu_3Si_2, the temperature dependence of $\rho(T)$ at various fields up to 0.4 T are measured [inset of Fig. 3(b)]. The T_c shifts to lower temperature and the ΔT_c broadens slightly with increasing field. At $\mu_0 H = 0.4$ T, the superconducting transition cannot be observed above 2 K. When defining the T_c as 50% drop from normal state resistivity just above superconducting transition, the temperature dependence of $\mu_0 H_{c2}(T)$ for YRu_3Si_2 is plotted in Fig. 3(b). Using the G-L formula $\mu_0 H_{c2}(T) = \mu_0 H_{c2}(0)(T_{c,0}^2 - T^2)/(T_{c,0}^2 + T^2)$, where $\mu_0 H_{c2}(0)$ is the zero-temperature upper critical field and $T_{c,0}$ is superconducting transition temperature at zero field. The fit (green line) gives $\mu_0 H_{c2}(0) = 0.78(2)$ T. On the other hand, when using the one-band Werthamer–Helfand–Hohenberg (WHH) formula (purple line),[40] the fitted $\mu_0 H_{c2}(0)$ is 0.655(2) T, close to the value obtained from the G-L formula. It is lower than that of $LaRu_3Si_2$ ($\mu_0 H_{c2}(0) \approx 4$ T).[32] In addition, the $\mu_0 H_{c2}(0)$ is also much smaller than the Pauli paramagnetically limited field $\mu_0 H_{c2}^p$ ($= 1.84\,T_c = 5.52$ T),[41] indicating that the orbital pairing-broken mechanism is dominant in YRu_3Si_2.

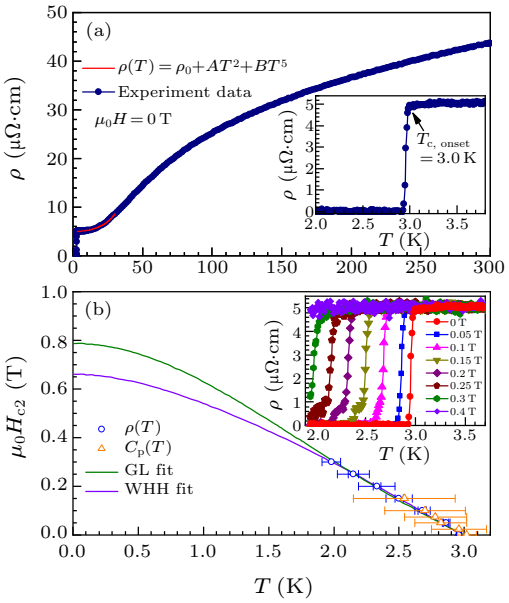

Fig. 3. (a) Temperature dependence of electrical resistivity $\rho(T)$ for YRu_3Si_2 polycrystal at zero field. The red solid line represents the fit using the formula $\rho(T) = \rho_0 + AT^2 + BT^5$. Inset: enlarged view of $\rho(T)$ curve near superconducting transition. (b) Temperature dependence of $\mu_0 H_{c2}(T)$. The blue circles and orange triangles represent the $\mu_0 H_{c2}(T)$ determined from resistivity and specific heat measurements, respectively. The error bars for the former are determined from the 10% and 90% of normal state resistivity just above superconducting transition. The error bars for the later are determined from the starting points and peak positions of jumps on the $C_p(T)$ curves. The green and purple lines represent the fits using the G-L and WHH formulas. Inset: $\rho(T)$ as a function of T at various magnetic fields.

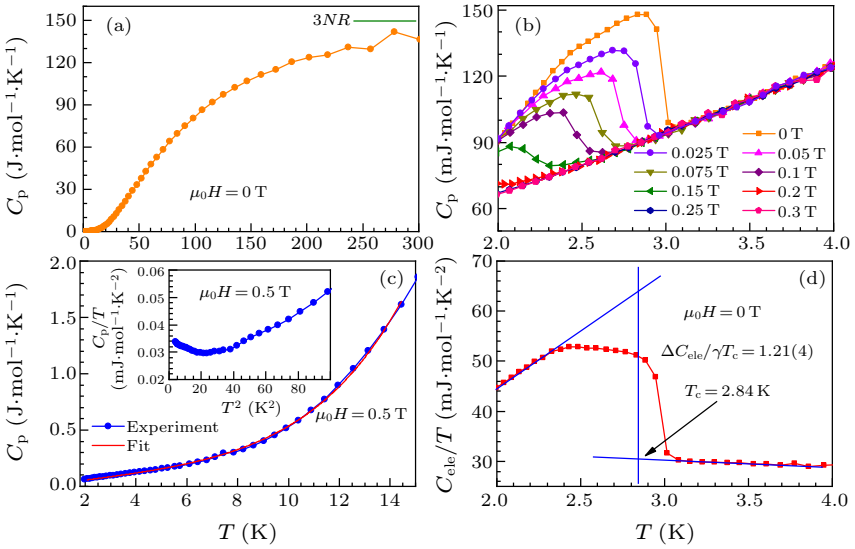

Fig. 4. (a) Temperature dependence of zero-field $C_p(T)$ from 300 K to 2 K. (b) C_p vs T at various magnetic fields. (c) Temperature dependence of $C_p(T)$ at $\mu_0 H = 0.5$ T. The red solid line represents the fit using the formula $C_p = \gamma T + \beta T^3 + \eta T^5$. Inset: C_p/T vs T^2 at $\mu_0 H = 0.5$ T. (d) C_{ele}/T as a function of T at zero field.

Using the fitted values of $\mu_0 H_{c1}(0)$ (= 28.0(3) mT) and $\mu_0 H_{c2}(0)$ (= 0.655(2) T), the zero-temperature superconducting characteristic parameters ξ_{GL} (coherence length) and λ_{GL} (penetration depth) can be estimated according to the following two equations $\xi_{GL} = (\frac{\phi_0}{2\pi\mu_0 H_{c2}(0)})^{1/2}$ and $\mu_0 H_{c1} = \frac{\phi_0}{4\pi\lambda_{GL}^2} \ln \frac{\lambda_{GL}}{\xi_{GL}}$, where ϕ_0 is the magnetic flux quantum ($h/2e = 2.07 \times 10^{-15}$ T·m^2). The calculated value of ξ_{GL} and λ_{GL} is 22.43(2) nm and 24.80(3) nm, respectively. Correspondingly, the derived GL parameter κ_{GL} ($= \lambda_{GL}/\xi_{GL}$) is 1.11(4), which is larger than $1/\sqrt{2}$. It confirms that YRu_3Si_2 is a type-Ⅱ superconductor. The zero-temperature thermodynamic critical field $\mu_0 H_c(0)$ is obtained to be 0.42(9) T using the equation $\mu_0 H_c(0) = [\mu_0 H_{c1}(0)\mu_0 H_{c2}(0)/\ln \kappa_{GL}]^{1/2}$.

Figure 4(a) shows the specific heat $C_p(T)$ of YRu_3Si_2 measured from 300 K to 2 K at zero field. At high temperature, consistent with the Dulong–Petit law, the $C_p(T)$ is close to the value of $3NR$ ($\sim$150 J·mol^{-1}·K^{-1}), where N (= 6) is the atomic numbers per formula and R (= 8.314 J·mol^{-1}·K^{-1}) is the ideal gas constant, respectively. At low temperature, a specific heat jump can be observed clearly due to the superconducting transition. It also confirms the bulk nature of superconductivity in YRu_3Si_2 [Fig. 4(b)]. With increasing field, this jump shifts to lower temperature accompanied with the decrease of height. On the other hand, at $\mu_0 H = 0.5$ T, where the superconducting transition is suppressed below 2 K, the relationship of C_p/T and T^2 cannot be described by a linear behavior [inset of Fig. 4(c)] and this suggests that there may be an anomalous contribution of high-frequency phonons.[32] Thus, the low-temperature $C_p(T)$ at $\mu_0 H = 0.5$ T is fitted using the formula $C_p = \gamma T + \beta T^3 + \eta T^5$, where the first item is the specific heat of electrons at normal state with the Sommerfeld coefficient γ, and the last two items represent the lattice specific heat when considering the contribution of high-frequency phonons.[42] The fit gives $\gamma = 27.5(8)$ mJ·mol^{-1}·K^{-2}, $\beta = 0.12(2)$ mJ·mol^{-1}·K^{-4} and $\eta = 0.00141(7)$ mJ·mol^{-1}·K^{-6}. By using the formula $\Theta_D = (12\pi^4 NR/5\beta)^{1/3}$, the calculated Debye temperature Θ_D is 460(26) K. It is larger than the value in $LaRu_3Si_2$ ($\Theta_D = 412$ K) derived using the same method,[32] possibly due to the smaller atomic mass of Y than La.

The specific heat of electrons C_{ele} can be obtained by subtracting the phonon contribution from the total specific heat [Fig. 4(d)] and the phonon contribution is obtained from the fit of $C_p(T)$ curve measured at 0.5 T. According to the method of equal-entropy construction (blue solid lines), the thermodynamic T_c is determined to be 2.84 K, consistent with the values obtained from the $\rho(T)$ and $\chi(T)$ curves. In addition, the determined $\mu_0 H_{c2}(T)$ from the $C_p(T)$ curves at various fields also exhibits similar trend when compared to the $\mu_0 H_{c2}(T)$ data derived from the resistivity measurements [orange triangles in Fig. 3(b)]. On the other hand, the specific heat jump $\Delta C_{ele}/\gamma T_c$ at T_c is 1.21(4), which is smaller than the value of weak-coupling limit 1.43. It implies that YRu_3Si_2 may be a weak- or moderate-coupling superconductor. It should be noted that the existence of Ru impurity could also contribute to the reduced specific heat jump. Using the obtained Θ_D and T_c, the electron-phonon coupling constant λ_{e-ph} can be calculated according to the McMillan equation[43]

$$\lambda_{e-ph} = \frac{1.04 + \mu^* \ln(\frac{\Theta_D}{1.45T_c})}{(1 - 0.62\mu^*)\ln(\frac{\Theta_D}{1.45T_c}) - 1.04}, \quad (1)$$

where μ^* is the Coulomb pseudopotential parameter. Taking $\mu^* = 0.13$ for many intermetallic superconductors, we can obtain the calculated value of λ_{e-ph} to be 0.50(2), further confirming that YRu_3Si_2 is a weak- or moderate-coupling superconductor. All of physical parameters of YRu_3Si_2 are listed in Table 1.

Table 1. Physical parameters of YRu_3Si_2 at superconducting and normal states.

Parameter	Units	Value
T_c	K	3.0
$\mu_0 H_{c1}(0)$	mT	28.0(3)
$\mu_0 H_{c2}(0)$	T	0.655(2)
$\mu_0 H_c(0)$	T	0.42(9)
ξ_{GL}	nm	22.43(2)
λ_{GL}	nm	24.80(3)
κ_{GL}		1.11(4)
$\Delta C_{ele}/\gamma T_c$		1.21(4)
λ_{e-ph}		0.50(2)
γ	mJ·mol^{-1}·K^{-2}	27.5(8)
Θ_D	K	460(26)
A/γ^2	μΩ·cm·mol^2·K^2·J^{-2}	3.15(2)
R_w		1.49(4)

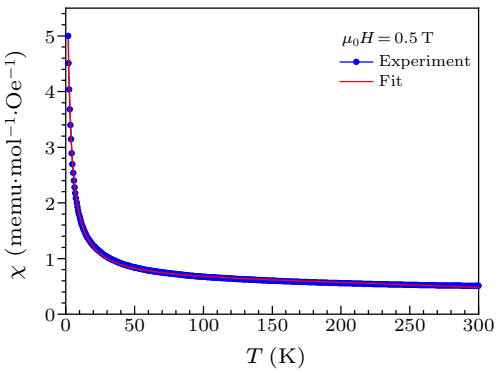

Fig. 5. Temperature dependence of $\chi(T)$ measured at $\mu_0 H = 0.5$ T with ZFC mode. The red solid line presents the fit using the formula $\chi(T) = \chi(0)[1 - (T/T_E)^2] + C/(T + T_0)$.

In order to get more information about electron correlation effect in YRu_3Si_2, temperature dependence of $\chi(T)$ at $\mu_0 H = 0.5$ T with ZFC mode is measured (Fig. 5). YRu_3Si_2 shows a paramagnetic behavior from 300 K to 2 K and no long-range magnetic translation is observed. In addition, it is found that the $\chi(T)$ curve can be well fitted using the following expression as in $LaRu_3Si_2$:[32]

$$\chi(T) = \chi(0)\left[1 - \left(\frac{T}{T_E}\right)^2\right] + \frac{C}{T + T_0}. \quad (2)$$

Here, the first term represents the Pauli susceptibility related to the density of state at the Fermi energy level

$E_{\rm F}$. The T_E represents a parameter proportional to the $E_{\rm F}$. The second term refers to the weak magnetic contribution that may be caused by the local moment. The fit gives $\chi(0) = 5.56(2) \times 10^{-4}\,\text{emu}\cdot\text{mol}^{-1}\cdot\text{Oe}^{-1}$, $T_{\rm E} = 640(10)\,\text{K}$, $C = 0.01393(7)\,\text{emu}\cdot\text{K}\cdot\text{mol}^{-1}\cdot\text{Oe}^{-1}$ and $T_0 = 1.38(2)\,\text{K}$. Using the fitted C, the calculated effective moment $\mu_{\rm eff}$ of YRu_3Si_2 is $0.3338(8)\,\mu_{\rm B}$/f.u., corresponding to $0.1113(3)\,\mu_{\rm B}$/Ru. This value is very close that in $LaRu_3Si_2$ ($0.105\,\mu_{\rm B}$/Ru)[33] and thus such Curie–Weiss behavior could be related to the existence of local moments of Ru atoms in YRu_3Si_2. On the other hand, the Kadawaki–Woods ratio A/γ^2 and the Wilson ratio $R_{\rm W} = 4\pi^2 k_{\rm B}^2 \chi(0)/3(g\mu_{\rm B})^2\gamma$ are often used to characterize the strength of electron correlations, where g is the Lande factor that takes about 2 for an electron and $\mu_{\rm B}$ is the Bohr magneton.[44,45] Using the above values of $A = 2.38(7) \times 10^{-3}\,\mu\Omega\cdot\text{cm}$, $\gamma = 27.5(8)\,\text{mJ}\cdot\text{mol}^{-1}\cdot\text{K}^{-2}$ and $\chi(0) = 5.56(2) \times 10^{-4}\,\text{emu}\cdot\text{mol}^{-1}\cdot\text{Oe}^{-1}$, the calculated A/γ^2 and the $R_{\rm w}$ are $3.15(2)\,\mu\Omega\cdot\text{cm}\cdot\text{mol}^2\cdot\text{K}^2\cdot\text{J}^{-2}$ and 1.49(4), respectively (summarized in Table 1). The value of A/γ^2 is much larger than those in transition metals ($0.4\,\mu\Omega\cdot\text{cm}\cdot\text{mol}^2\cdot\text{K}^2\cdot\text{J}^{-2}$) and relatively smaller than the universal value $10\,\mu\Omega\cdot\text{cm}\cdot\text{mol}^2\cdot\text{K}^2\cdot\text{J}^{-2}$ in heavy-fermion systems.[44,46] The value of $R_{\rm W}$ is larger than 1 that is expected in noninteracting free electron gas. Both large A/γ^2 and $R_{\rm W}$ suggest strong electron correlations in YRu_3Si_2.

In summary, kagome metal YRu_3Si_2 shows a superconducting transition at $T_{\rm c} \sim 3.0\,\text{K}$. The zero-temperature $\mu_0 H_{\rm c1}(0)$ and $\mu_0 H_{\rm c2}(0)$ is $28.0(3)\,\text{mT}$ and $0.655(2)\,\text{T}$, respectively. The derived $\kappa_{\rm GL}$ is 1.11(4), confirming that YRu_3Si_2 is a type-Ⅱ superconductor. Moreover, the relatively small $\Delta C_{\rm ele}/\gamma T_{\rm c}$ and $\lambda_{\rm e-ph}$ indicate that YRu_3Si_2 has a weakly or moderately coupled BCS bulk superconductivity. On the other hand, rather strong electron correlation effect is identified by the large values of A/γ^2 and $R_{\rm W}$. This could be related to the existence of kagome flat band in YRu_3Si_2, which can result in high density of states near the $E_{\rm F}$.

Acknowledgements. This work was supported by the National Key R&D Program of China (Grant No. 2018YFE0202600), the Beijing Natural Science Foundation (Grant No. Z200005), the Fundamental Research Funds for the Central Universities and Research Funds of Renmin University of China (RUC) (Grant Nos. 18XNLG14, 19XNLG13, 19XNLG17, and 22XNKJ40), and the Beijing National Laboratory for Condensed Matter Physics.

References

[1] Balents L 2010 *Nature* **464** 199
[2] Broholm C, Cava R J, Kivelson S A, Nocera D G, Norman M R and Senthil T 2020 *Science* **367** eaay0668
[3] Shores M P, Nytko E A, Bartlett B M and Nocera D G 2005 *J. Am. Chem. Soc.* **127** 13462
[4] Han T H, Helton J S, Chu S, Nocera D G, Rodriguez-Rivera J A, Broholm C and Lee Y S 2012 *Nature* **492** 406
[5] Ye L, Kang M, Liu J, von Cube F, Wicker C R, Suzuki T, Jozwiak C, Bostwick A, Rotenberg E, Bell D C, Fu L, Comin R and Checkelsky J G 2018 *Nature* **555** 638
[6] Kang M, Ye L, Fang S, You J S, Levitan A, Han M, Facio J I, Jozwiak C, Bostwick A, Rotenberg E, Chan M K, McDonald R D, Graf D, Kaznatcheev K, Vescovo E, Bell D C, Kaxiras E, van den Brink J, Richter M, Ghimire M P, Checkelsky J G and Comin R 2020 *Nat. Mater.* **19** 163
[7] Liu Z H, Li M, Wang Q, Wang G W, Wen C H P, Jiang K, Lu X L, Yan S C, Huang Y B, Shen D W, Yin J X, Wang Z Q, Yin Z P, Lei H C and Wang S C 2020 *Nat. Commun.* **11** 4002
[8] Kang M, Fang S, Ye L, Po H C, Denlinger J, Jozwiak C, Bostwick A, Rotenberg E, Kaxiras E, Checkelsky J G and Comin R 2020 *Nat. Commun.* **11** 4004
[9] Nakatsuji S, Kiyohara N and Higo T 2015 *Nature* **527** 212
[10] Nayak A K, Fischer J E, Sun Y, Yan B, Karel J, Komarek A C, Shekhar C, Kumar N, Schnelle W, Kübler J, Felser C and Parkin S S P 2016 *Sci. Adv.* **2** e1501870
[11] Wang Q, Sun S S, Zhang X, Pang F and Lei H C 2016 *Phys. Rev. B* **94** 075135
[12] Liu E, Sun Y, Kumar N, Muechler L, Sun A, Jiao L, Yang S Y, Liu D, Liang A, Xu Q, Kroder J, Süß V, Borrmann H, Shekhar C, Wang Z, Xi C, Wang W, Schnelle W, Wirth S, Chen Y, Goennenwein S T B and Felser C 2018 *Nat. Phys.* **14** 1125
[13] Wang Q, Xu Y F, Lou R, Liu Z H, Li M, Huang Y B, Shen D W, Weng H M, Wang S C and Lei H C 2018 *Nat. Commun.* **9** 3681
[14] Yin J X, Zhang S S, Li H, Jiang K, Chang G, Zhang B, Lian B, Xiang C, Belopolski I, Zheng H, Cochran T A, Xu S Y, Bian G, Liu K, Chang T R, Lin H, Lu Z Y, Wang Z, Jia S, Wang W and Hasan M Z 2018 *Nature* **562** 91
[15] Yin J X, Ma W, Cochran T A, Xu X, Zhang S S, Tien H J, Shumiya N, Cheng G, Jiang K, Lian B, Song Z, Chang G, Belopolski I, Multer D, Litskevich M, Cheng Z J, Yang X P, Swidler B, Zhou H, Lin H, Neupert T, Wang Z, Yao N, Chang T R, Jia S and Hasan M Z 2020 *Nature* **583** 533
[16] Ortiz B R, Gomes L C, Morey J R, Winiarski M, Bordelon M, Mangum J S, Oswald I W H, Rodriguez-Rivera J A, Neilson J R, Wilson S D, Ertekin E, McQueen T M and Toberer E S 2019 *Phys. Rev. Mater.* **3** 094407
[17] Ortiz B R, Teicher S M L, Hu Y, Zuo J L, Sarte P M, Schueller E C, Abeykoon A M M, Krogstad M J, Rosenkranz S, Osborn R, Seshadri R, Balents L, He J F and Wilson S D 2020 *Phys. Rev. Lett.* **125** 247002
[18] Ortiz B R, Sarte P M, Kenney E M, Graf M J, Teicher S M L, Seshadri R and Wilson S D 2021 *Phys. Rev. Mater.* **5** 034801
[19] Yin Q W, Tu Z J, Gong C S, Fu Y, Yan S H and Lei H C 2021 *Chin. Phys. Lett.* **38** 037403
[20] Ko W H, Lee P A and Wen X G 2009 *Phys. Rev. B* **79** 214502
[21] Wang W S, Li Z Z, Xiang Y Y and Wang Q H 2013 *Phys. Rev. B* **87** 115135
[22] Kiesel M L, Platt C and Thomale R 2013 *Phys. Rev. Lett.* **110** 126405
[23] Mazin I I, Jeschke H O, Lechermann F, Lee H, Fink M, Thomale R and Valentí R 2014 *Nat. Commun.* **5** 4261
[24] Jiang Y X, Yin J X, Denner M M, Shumiya N, Ortiz B R, He J, Liu X, Zhang S S, Chang G, Belopolski I, Zhang Q, Hossain M S, Cochran T A, Multer D, Litskevich M, Cheng Z J, Yang X P, Guguchia Z, Xu G, Wang Z, Neupert T, Wilson S D and Hasan M Z 2021 *Nat. Mater.* **20** 1353
[25] Chen H, Yang H, Hu B, Zhao Z, Yuan J, Xing Y, Qian G, Huang Z, Li G, Ye Y, Yin Q, Gong C, Tu Z, Lei H, Ma S, Zhang H, Ni S, Tan H, Shen C, Dong X, Yan B, Wang Z and Gao H J 2021 *Nature* **599** 222

[26] Rapp Ö, Invarsson J and Claeson T 1974 *Phys. Lett. A* **50** 159
[27] Sun S S, Liu K and Lei H C 2016 *J. Phys.: Condens. Matter* **28** 085701
[28] Gong C S, Wang Q, Wang S H and Lei H C 2020 *J. Phys.: Condens. Matter* **32** 295601
[29] Ku H C, Meisner G P, Acker F and Johnston D C 1980 *Solid State Commun.* **35** 91
[30] Barz H 1980 *Mater. Res. Bull.* **15** 1489
[31] Escorne M, Mauger A, Gupta L C and Godart C 1994 *Phys. Rev. B* **49** 12051
[32] Li S, Zeng B, Wan X G, Tao J, Han F, Yang H, Wang Z H and Wen H H 2011 *Phys. Rev. B* **84** 214527
[33] Li B X, Li S and Wen H H 2016 *Phys. Rev. B* **94** 094523
[34] Mielke III C, Qin Y, Yin J X, Nakamura H, Das D, Guo K, Khasanov R, Chang J, Wang Z Q, Jia S, Nakatsuji S, Amato A, Luetkens H, Xu G, Hasan M Z and Guguchia Z 2021 *Phys. Rev. Mater.* **5** 034803
[35] Vandenberg J M and Barz H 1980 *Mater. Res. Bull.* **15** 1493
[36] TOPAS Version 4; Bruker AXS, Karlsruhe, Germany (2007).
[37] Aharoni A 1998 *J. Appl. Phys.* **83** 3432
[38] Ioffe A F and Regel A R 1961 *Prog. Semicond.* **4** 237
[39] Zverev V N, Korobenko A V, Sun G L, Sun D L, Lin C T and Boris A V 2009 *JETP Lett.* **90** 130
[40] Werthamer N R, Helfand E and Hohenberg P C 1966 *Phys. Rev.* **147** 295
[41] Maki K 1966 *Phys. Rev.* **148** 362
[42] Yang H D and Lin J Y 2001 *J. Phys. Chem. Solids* **62** 1861
[43] McMillan W L 1968 *Phys. Rev.* **167** 331
[44] Kadowaki K and Woods S B 1986 *Solid State Commun.* **58** 507
[45] Wilson K G 1975 *Rev. Mod. Phys.* **47** 773
[46] Jacko A C, Fjærestad J O and Powell B J 2009 *Nat. Phys.* **5** 422